

# Spatial propagation of COVID-19 across the United States

Nick James and Howard Bondell

*School of Mathematics and Statistics,  
University of Melbourne, Victoria 3010, Australia*

Max Menzies\*

*Yau Mathematical Sciences Center,  
Tsinghua University, Beijing 100084, China*

(Dated: May 17, 2022)

## Abstract

This paper introduces a novel approach to spatio-temporal data analysis using metric geometry to study the spatial propagation of COVID-19 across the United States and reveal periods when the change in geographic distribution was most profound. Using a spatially-defined geodesic Wasserstein metric, we analyze discrepancies between the density functions of new case counts on any given day, incorporating the geographic spread of cases. This methodology could provide new approaches and insights for analysts to monitor the spatial spread of epidemics and other events, and enable regional policymakers to protect their localities in advance.

COVID-19 remains an ongoing threat to the public health of the United States (US). While an aggressive vaccination program has reduced cases and deaths considerably from their highs in January 2021 [1], the vaccination rate is highly non-uniform across the country [2]. Communities with low vaccination rates remain a risk, to themselves, as well as to the rest of the nation, both regarding the spread of the virus to vulnerable people elsewhere and the potential for further virus mutation. Throughout the pandemic, the imposition of restrictions on community activity and businesses, including mask mandates and lockdowns, has mostly fallen to state and local governments. Thus, it remains of considerable interest to local lawmakers to track the ongoing spatial propagation of COVID-19 across the US. This may reveal trends in the spread of the virus, allow for forewarning before local outbreaks, identify locations that performed unusually well or poorly in containment measures, and provide opportunities to learn from other localities.

There are numerous existing analyses of the propagation of COVID-19 across the US on a state-by-state or finer basis. Previous research has used a variety of techniques, including state-by-state time series analysis [3, 4], SEIR models [5], regression models and feature selection [6, 7], Markov chain Monte Carlo models [8], and other Monte Carlo simulations [9]. Similar studies have been carried out in other countries, such as the United Kingdom [10], Brazil [11], and China [12], or comparing numerous countries simultaneously [13, 14]. Most of these studies are qualitatively descriptive in their summary of the spread of COVID-19 across the geography of a country. Prior physically-inspired research on COVID-19 has focused on fluids and aerosols [15–19], characteristics of optimal antigens [20], contagion and percolation models [21, 22] and network models [23–25]. Methods from statistical physics have been used widely to study both COVID-19 and prior epidemics [20, 25–27].

This paper introduces a new mathematical method for studying the spatial propagation of an epidemic over time. Our approach applies metric geometry to perform an in-depth analysis of the time-varying spatial distribution of COVID-19 cases across US states. Let  $(X, d)$  be any metric space,  $\mu, \nu$  two probability measures on  $X$ , and  $q \geq 1$ . The Wasserstein metric between  $\mu, \nu$  is defined as

$$W^q(\mu, \nu) = \inf_{\gamma} \left( \int_{X \times X} d(x, y)^q d\gamma \right)^{\frac{1}{q}}, \quad (1)$$

where the infimum is taken over all probability measures  $\gamma$  on  $X \times X$  with marginal distributions  $\mu$  and  $\nu$ . Henceforth, let  $q = 1$ . By the Kantorovich-Rubinstein formula [28], there is an alternative formulation when  $X$  is compact (for example, finite):

$$W^1(\mu, \nu) = \sup_F \left| \int_X F d\mu - \int_X F d\nu \right|, \quad (2)$$

where the supremum is taken over all 1-Lipschitz functions  $F : X \rightarrow \mathbb{R}$ .

Throughout this paper, let  $X$  be the set of the 50 US states and the District of Columbia (DC), ordered alphabetically and indexed  $i = 1, \dots, 51$ . As this is a finite set, measures  $\mu, \nu$  may be reinterpreted as probability vectors  $f, g \in \mathbb{R}^{51}$  such that  $f_i \geq 0$  and  $\sum_{i=1}^{51} f_i = 1$ . Such probability vectors are our central object of study, as they define the spatial distribution over the US. The simplest metric we can equip  $X$  with is the discrete metric, where  $d(x, y) = 1$  if  $x \neq y$ , and 0 otherwise. In this case, the formulation (2) of Wasserstein metric is optimized with the choice of function

$$F(x) = \begin{cases} 1, & f(x) \geq g(x), \\ 0, & f(x) < g(x), \end{cases} \quad (3)$$

and thus greatly simplifies to a relatively simple metric

$$W_{disc}(f, g) = \frac{1}{2} \|f - g\|_1. \quad (4)$$

A proof of this statement is included in the appendix. We refer to this as the *discrete Wasserstein distance* - it will not be our primary object of study but will be utilized later to demonstrate the robustness of our results.

Our primary mathematical contribution is obtained by setting the metric  $d$  on  $X$  to be the real-world geodesic distances between (the centroids of) the 50 US states and DC, measured in meters. We term the associated Wasserstein distance the *geodesic Wasserstein distance* and notate it as  $W_G(f, g)$  for two probability vectors  $f, g$ .

Consider the illustrative case where  $f$  and  $g$  are Dirac delta functions supported on single elements  $x$  and  $y$ , respectively. By the formulation (2), it follows that  $W^1(f, g) = d(x, y)$ . For the discrete Wasserstein distance, this means that  $W_{disc}(f, g) = 1$  if  $x \neq y$ , whereas  $W_G(f, g)$  is the physical distance between (the centroids of the) states indexed by  $x$  and  $y$ . Thus, the geodesic Wasserstein distance allows us to factor in the physical spread of COVID-19 across the US. That is, the discrete Wasserstein distance (or  $L^1$  norm) between probability vectors does not take into account distance between states; the geodesic Wasserstein awards a greater distance between two probability vectors if the proportion of cases has shifted further away geographically.

We use this new metric for two aims. First, we wish to determine the periods with the most rapid change in spatial propagation of COVID-19 across the US. Second, we investigate whether there is any reversion behavior in this spatial propagation. While existing studies have typically analyzed the behavior of the different waves of the pandemic on a state-by-state basis, our approach will identify distinct times where a similar geographic distribution of COVID-19 returned across the US. In doing so, it can identify similarities in successive waves of the pandemic.

Our data spans March 12, 2020 to June 30, 2021 across  $n = 51$  states and DC, a period of  $T = 476$  days. We begin here to avoid periods of sparse reporting early in the pandemic. In order to reduce irregularities in daily counts, such as lower reporting of tests on weekends, we first apply a simple 7-day smoothing operator to the counts. This yields a multivariate time series of smoothed new cases  $x_i(t), i = 1, \dots, n, t = 1, \dots, T$ . For the first experiment, we consider grouped probability vectors of 30-day periods. Specifically, let  $f^{[a:b]}$  be the probability vector of (smoothed) new cases in each state, observed across an interval  $a \leq t \leq b$ , divided by the total number of US cases across this period:

$$f_i^{[a:b]} = \frac{\sum_{t=a}^b x_i(t)}{\sum_{t=a}^b \sum_{j=0}^n x_j(t)}, i = 0, \dots, n. \quad (5)$$

When  $a = b$ , we simply notate this as  $f_i(t)$ . In Figure 1, we display the distance function

$$t \mapsto W_G(f^{[t-30:t-1]}, f^{[t:t+29]}), \quad 31 \leq t \leq T - 29, \quad (6)$$

between adjacent 30-day periods. For example,  $t = 51$  corresponds to May 1, and the associated function value is the geodesic Wasserstein distance between the probability vector of cases across April 1-30 and May 1-30. Within this figure, we also notate local maxima (over a 30-day window).

The primary finding of this figure is a drastic peak on June 6, 2020. This reveals that the spatial distribution of cases throughout the month of May (broadly speaking) was significantly different to that throughout the month of June. Other more moderate peaks are observed on August 23, 2020, December 6, 2020, March 5, 2021, and May 30, 2021. Throughout the figure, the function (6) consistently displays rather regular patterns of increase and decrease. To complement our primary finding, we take a deeper analysis of the 30-day periods prior to and following our peak date, June 6, 2020.

The primary difference between the spatial distribution of COVID-19 cases across the US during the months of May and June 2020 is that May was dominated by high numbers of new cases in the Northeastern states, while cases spread much wider in June, impacting larger states such as California, Texas and Florida with significant case counts. We elucidate and quantify this with an individual state-by-state analysis of the distributional changes between May and June.

In Figure 2, we plot the time-varying probability densities  $f_i(t)$  for select states over the period May 7, 2020 to July 5, 2020. These figures show the substantial change in the distribution of COVID-19 across the country during this 60-day period. In Figures 2a, 2b, 2c, 2d respectively, we see that four Northeastern states, New York, New Jersey, Massachusetts, and Pennsylvania exhibit a considerable decline in this period in their proportion of the total new COVID-19 cases across the US. While not a Northeastern state, the similarly urbanized and politically inclined state of Illinois (2e) also exhibits a drastic decline. On the other hand, California (2f), Texas (2g), Florida (2h) and Arizona (2i) exhibit a considerable increase. Altogether, Figure 2 shows the decline in the densities in the Northeastern states and the relative increase in all other areas of the country in the month of June.

We provide more quantitative detail in Table I, where we compute normalized integrals of

the time-varying daily density function  $f_i(t)$  for each state between May 7 to June 5 and June 6 to July 5. That is, we compute the following for each state, expressed as a percentage:

$$\Delta(f)_i = \frac{1}{30} \sum_{t=t_0}^{t_0+29} f_i(t) - \frac{1}{30} \sum_{t=t_0-30}^{t_0-1} f_i(t). \quad (7)$$

The states with the largest absolute changes in their average percentage of US total new cases are Florida (increase of 7.59), Texas (increase of 6.25), Illinois (decrease of 6.08), New York (decrease of 5.42), Arizona (increase of 5.00), California (increase of 4.57), New Jersey and Massachusetts (decreases of 3.53 and 3.48 respectively). Across all states, the sum of the absolute value of the changes in average proportion is 67.86%. As this coincides with an  $L^1$  norm between distributions, we deduce that  $W_{disc}(f^{[t_0-30:t_0-1]}, f^{[t_0:t_0+29]}) = 0.3393$ , by (4). This is a substantial difference (its maximal possible difference is 1), and validates the sizeable change in the distribution of cases between these two 30-day periods.

We complete this first analysis with a novel mathematical approach to quantify the spread of a probability distribution across a metric space, while taking the spatial structure into account. Given a distribution  $f$  corresponding to a measure  $\mu$  on a finite metric space  $(X, d)$ , let

$$\text{Var}(f) = \int_{X \times X} d(x, y)^2 d\mu(x) d\mu(y) = \sum_{x, y \in X} d(x, y)^2 f(x) f(y), \quad (8)$$

where the second equality is valid when the metric space is discrete, as in this example. We term (8) the *geodesic variance* of the distribution  $f$ . We explain how this is a generalization of the classic notion of variance in the appendix.

The geodesic variance is zero for a Dirac delta  $f = \delta_x$ , and greater when the distribution is more spread out across the space. In Figure 3, we plot the time-varying variance of grouped 30-day distributions,  $t \mapsto \text{Var}(f^{[t:t+29]})$ . This figure reveals that the geographic variance of COVID-19 across the US is globally minimal when  $t$  corresponds to May 3, 2020, reflecting the 30-day period until June 1, 2020. From this point, it sharply increases, corresponding to the spread of the virus across the country, complementing the findings already observed.

For our second aim, we investigate the extent of spatial reversion over time. We wish to identify, for some values of  $t$ , is there a non-trivial similarity with subsequent times  $s > t$ . For each  $t$ , we consider intervals  $\{s : s \geq t + 30\}$  to avoid trivial similarity

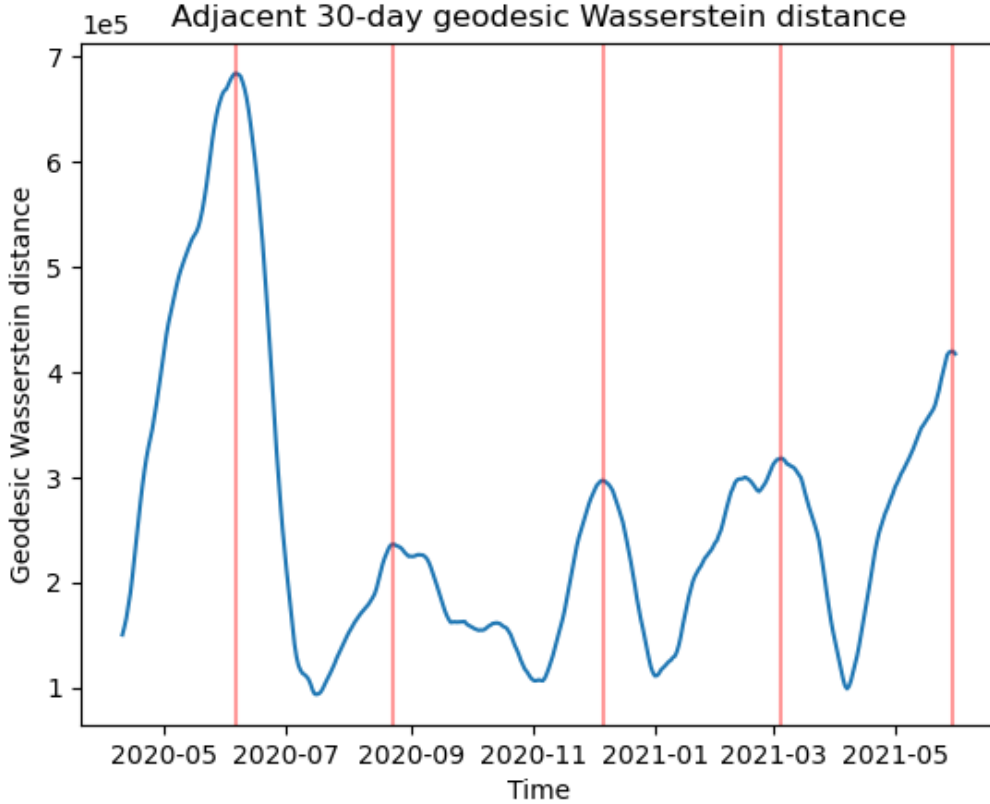


FIG. 1: Time-varying geodesic Wasserstein distance (in meters) between adjacent aggregated 30-day distributions of new cases. Large spikes in this distance indicate meaningful shifts in the spatial distribution of COVID-19 over a one-two month transition. The large first peak corresponds to June 6, 2020, signifying that the prior and proceeding 30-day periods have substantially different spatial distributions. The prior 30 days (May 7 to June 5) are characterized by the dominance of Northeastern states, while the proceeding 30 days (June 6 to July 5) are characterized by the ascent of case numbers elsewhere, including California, Texas, Florida and Arizona.

with neighbouring times and record both  $\min\{W_G(f^{[s:s+29]}, f^{[t:t+29]}) : s \geq t + 30\}$  and  $\operatorname{argmin}\{W_G(f^{[s:s+29]}, f^{[t:t+29]}) : s \geq t + 30\}$ . Ignoring the trivial region of being within 30 days of  $t$ , these determine the time  $s$  whose COVID-19 distribution is most similar to time  $t$  as well as the magnitude of that similarity. We plot both the  $\operatorname{argmin}$  function, in days, and the  $\min$  function, in meters, in Figure 4a. To provide more details, we also plot  $W_G(f^{[s:s+29]}, f^{[t:t+29]})$  for all non-trivial values of  $s \geq t + 30$  in Figure 4b.

We see two main findings in these figures. In Figure 4a, non-trivial spatial reversion is characterized by the  $\operatorname{argmin}$  function being greater than 30 (the nearest permissible day under consideration). With this in mind, two main findings are observed. First, April 2020 has both

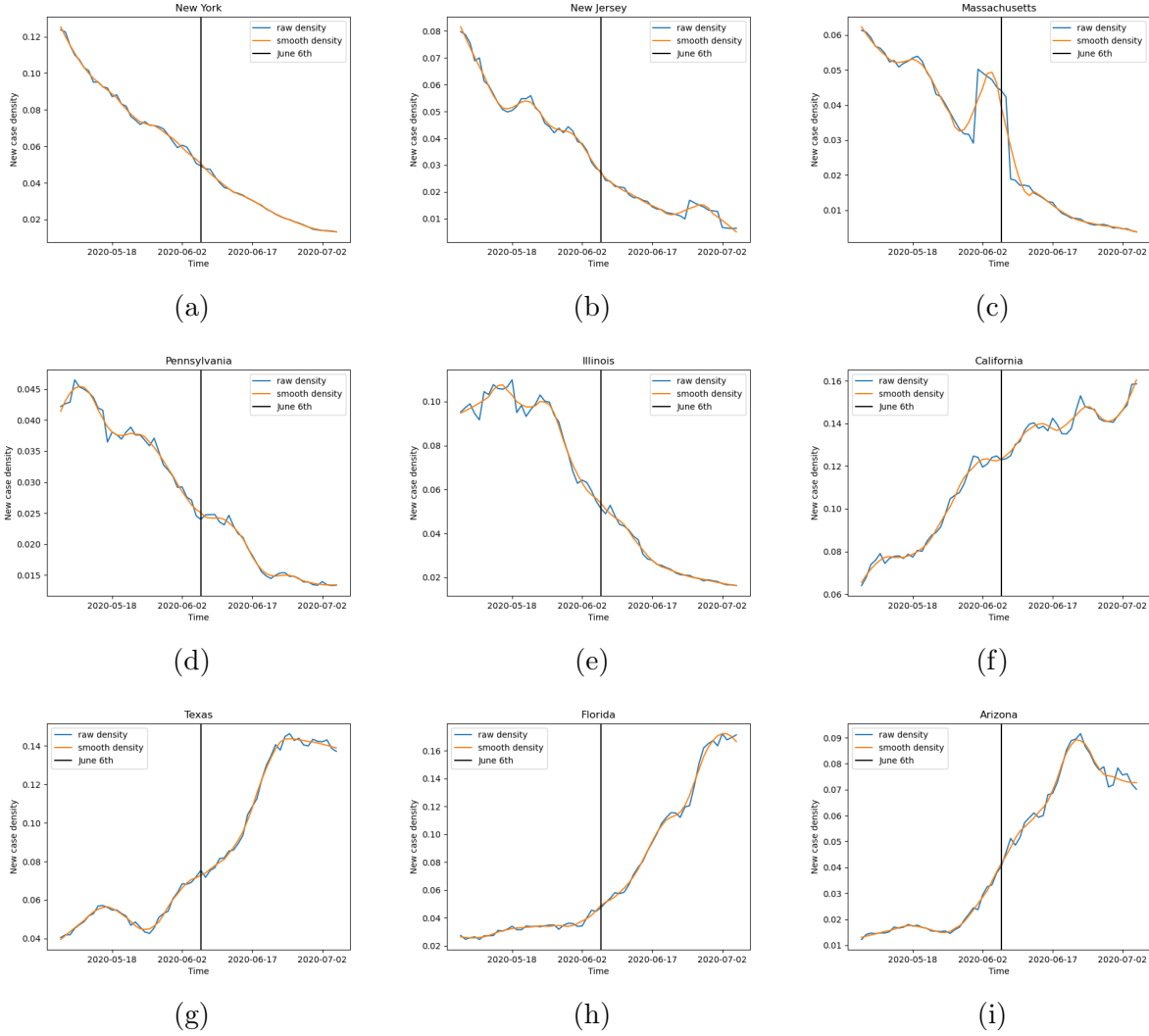


FIG. 2: Time-varying densities of new cases for (a) New York (b) New Jersey (c) Massachusetts (d) Pennsylvania (e) Illinois (f) California (g) Texas (h) Florida (i) Arizona across the period May 7 to July 5, 2020. This 60-day interval was identified in Figure 1 as the most substantial period of geographic change in the entire period.

a high min and argmin, seen in Figure 4a. The value of the argmin is 350 days, revealing maximal proximity to a period about one year later; the value of the min is approximately 400 km. Thus, this period is not very similar to any other period, but it is weakly similar to April 2021. April 2020 is characterized by the early dominance of the Northeastern US states. This reflects that this period was quite distinct from any other time, but that April 2021 reflects a weak reemergence of the Northeast as significant contributor to the nation’s cases.

Secondly, June 2020 is characterized by a relatively low value in the minimum, revealing substantial non-trivial similarity to a subsequent period. The argmin here is approximately



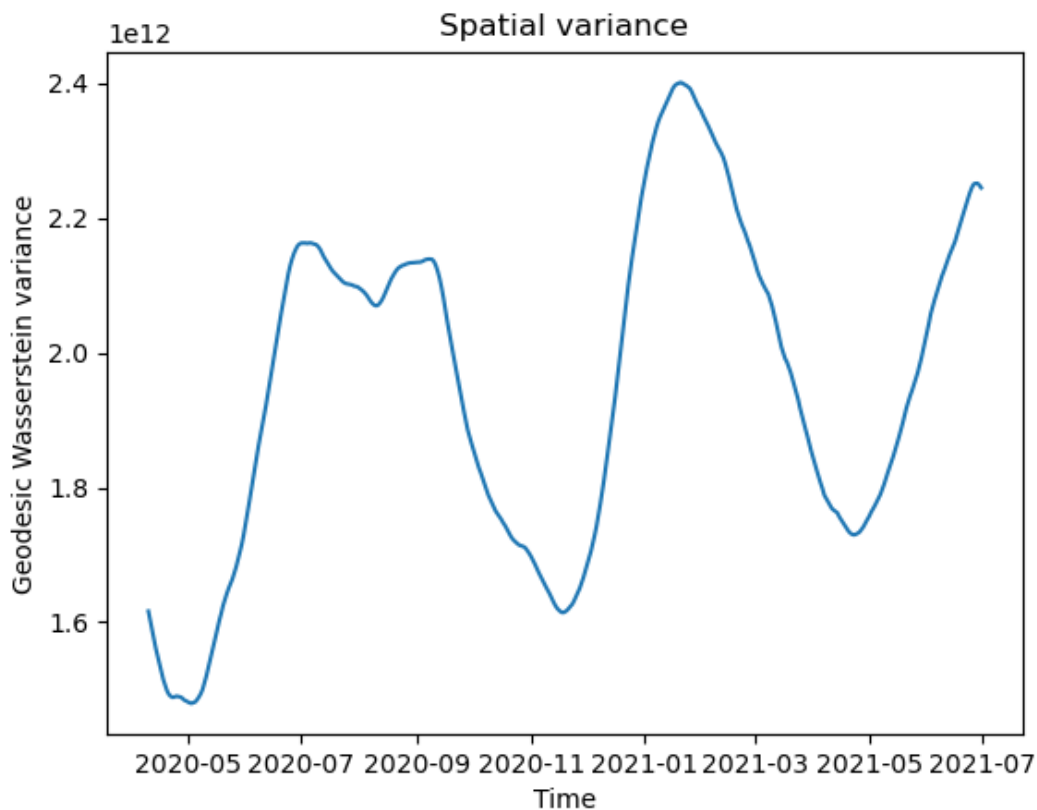
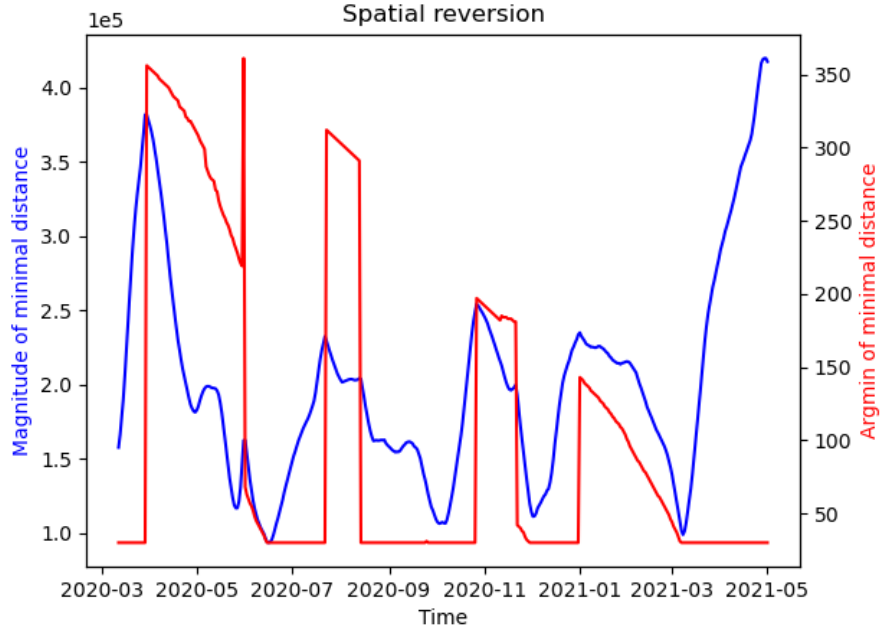


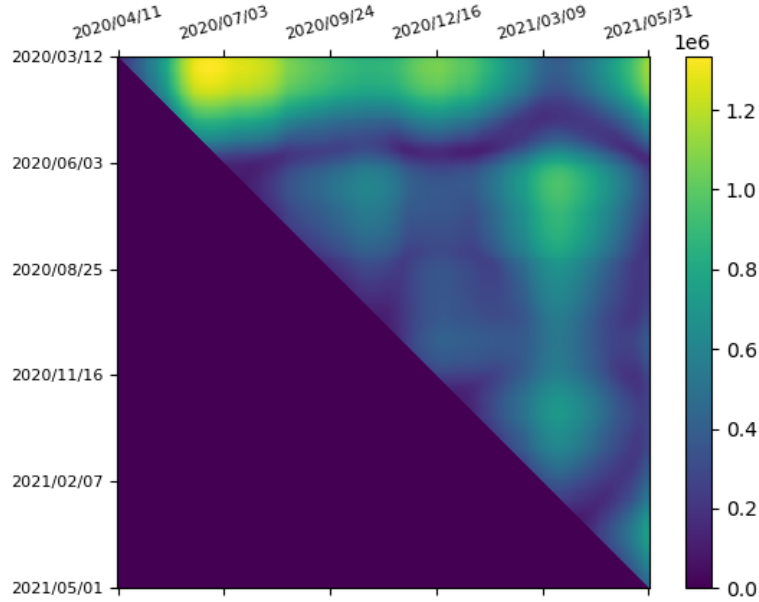
FIG. 3: Time-varying geodesic variance (in square meters) (8) of 30-day aggregated distributions. The global minimum at May 3, 2020 reflects the spatial concentration of new COVID-19 cases in the Northeastern states during the period May 3 to June 1. In the proceeding 30 days, the geodesic variance grows considerably as new cases become much more spread across the US.

200 days and then immediately after about 360 days. This reflects that June 2020 is highly similar to the period comprising December 2020 and January 2021, as well as the period of June 2021. Indeed, June 2020 is characterized by the second wave of COVID-19 in the US overall, and the first wave in large states California, Texas and Florida, while the beginning of 2021 is characterized by the third wave of COVID-19 in the US overall, and the second wave in the aforementioned large states. The sudden increase in the argmin function around this date reveals additional similarity with June 2021, in which a fourth wave of COVID-19 in the US is beginning. That is, the argmin values around June 2020 reveal two different subsequent reversions in the geographic distribution of COVID-19. This strong similarity is also visible in the darker regions of Figure 4b, to the right of the  $y$ -value of  $t$  as June 1, 2020.

In conclusion, we have introduced a new methodological framework to analyze the spatio-



(a)



(b)

FIG. 4: Spatial reversion of the distribution of COVID-19 cases over time. In (a), we plot both the argmin, in days, and the size of the minimal value, in meters, of  $\{W_G(f^{[s:s+29]}, f^{[t:t+29]}) : s \geq t + 30\}$  as  $t$  varies. Periods where the argmin is greater than 30 indicates non-trivial spatial reversion occurs at a time later than  $t$ . April 2020 is revealed to be weakly similar to a year in the future, but not to any other time. June 2020 is revealed to be similar to both January 2021 and June 2021. In (b), we plot  $W_G(f^{[s:s+29]}, f^{[t:t+29]})$  for all non-trivial values  $s \geq t + 30$ . Substantial similarity between June 2020 and various later times are visible in the darker band to the top right of the figure.

State	$\Delta(f)_i$	State	$\Delta(f)_i$
Alabama	0.82	Montana	0.04
Alaska	0.06	Nebraska	-0.70
Arizona	5.00	Nevada	0.62
Arkansas	0.93	New Hampshire	-0.19
California	4.57	New Jersey	-3.53
Colorado	-0.75	New Mexico	-0.09
Connecticut	-1.41	New York	-5.42
Delaware	-0.41	North Carolina	1.58
District of Columbia	-0.38	North Dakota	-0.10
Florida	7.59	Ohio	-0.51
Georgia	1.09	Oklahoma	0.42
Hawaii	0.03	Oregon	0.30
Idaho	0.22	Pennsylvania	-1.89
Illinois	-6.08	Rhode Island	-0.58
Indiana	-0.94	South Carolina	1.96
Iowa	-0.46	South Dakota	-0.15
Kansas	-0.17	Tennessee	0.62
Kentucky	-0.04	Texas	6.25
Louisiana	0.59	Utah	0.70
Maine	-0.07	Vermont	0.01
Maryland	-2.53	Virginia	-1.91
Massachusetts	-3.48	Washington	0.23
Michigan	-0.65	West Virginia	-0.02
Minnesota	-1.36	Wisconsin	-0.09
Mississippi	0.13	Wyoming	0.02
Missouri	0.24		

TABLE I: US states and their values of  $\Delta(f)_i$ , defined in (7), measuring the percentage change in their contribution to new US cases between the adjacent 30-day periods of May 7 to June 5 and June 6 to July 5, 2020.

temporal propagation of a process, such as an epidemic across a physical region. Future work could modify our framework, replacing geographical distance with other notions of proximity. For example, one could consider two locations as close, assigning them a low measure of distance, if there is substantial travel between them. Our methodology could be combined with existing methods of network analysis, or applied on a more granular basis to individual US counties.

COVID-19 data is sourced from the New York Times [29] and US location data is sourced from Google [30].

## Appendix

**Proposition 1.** *Let  $(X, d)$  be a finite discrete metric space, with  $d(x, y) = 1$  for all  $x \neq y$  and zero otherwise. Let  $W^1(\mu, \nu)$  be the  $L^1$ -Wasserstein metric between two probability measures  $\mu, \nu$  on  $X$ , with corresponding distribution functions  $f, g$ , expressed as in (2). That is,*

$$W^1(\mu, \nu) = \sup_F \left| \int_X F d\mu - \int_X F d\nu \right|. \quad (9)$$

*Then, this supremum is optimized by the choice of  $F$  as in (3), namely*

$$F(x) = \begin{cases} 1, & f(x) \geq g(x), \\ 0, & f(x) < g(x). \end{cases} \quad (10)$$

*As such,  $W^1(f, g)$  reduces to the simple form of (4), namely*

$$W^1(f, g) = \frac{1}{2} \|f - g\|_1. \quad (11)$$

*Proof.* Let  $F$  be an arbitrary 1-Lipschitz function on  $X$ . That is,  $F : X \rightarrow \mathbb{R}$  and  $|F(x) - F(y)| \leq d(x, y) = 1$  for  $x \neq y$ . Let  $M = \sup_{x \in X} F(x)$ ,  $m = \inf_{y \in X} F(y)$ . By taking the supremum over  $x$  and the infimum over  $y$ , the Lipschitz condition ensures that  $M - m \leq 1$ .

So

$$\int_X F d\mu - \int_X F d\nu = \sum_{x \in X} F(x)(f(x) - g(x)) \quad (12)$$

$$\leq \sum_{x:f(x) \geq g(x)} M(f(x) - g(x)) + \sum_{x:f(x) < g(x)} m(f(x) - g(x)) \quad (13)$$

$$\leq \sum_{x:f(x) \geq g(x)} (m+1)(f(x) - g(x)) + \sum_{x:f(x) < g(x)} m(f(x) - g(x)) \quad (14)$$

$$= \sum_{x:f(x) \geq g(x)} f(x) - g(x) + \sum_{x \in X} m(f(x) - g(x)) \quad (15)$$

$$= \sum_{x:f(x) \geq g(x)} f(x) - g(x), \quad (16)$$

using the fact that  $\sum_x f(x) = \sum_x g(x) = 1$  to eliminate the second sum. Now, let

$$P = \sum_{x:f(x)\geq g(x)} f(x) - g(x), \quad (17)$$

$$N = \sum_{x:f(x)<g(x)} g(x) - f(x). \quad (18)$$

Then  $P - N = \sum_{x\in X} f(x) - g(x) = 0$ , while  $P + N = \sum_{x\in X} |f(x) - g(x)| = \|f - g\|_1$ . Thus, we deduce  $P = N = \frac{1}{2}\|f - g\|_1$ , and  $|\int_X F d\mu - \int_X F d\nu| \leq P$ . Taking the supremum over  $F$ , we deduce  $W^1(f, g) \leq P$ . Finally, let  $F$  be as in (10). Then  $\int_X F d\mu - \int_X F d\nu$  immediately coincides with  $P$ , by definition. Thus, the supremal value coincides with  $P$ , and  $P = \frac{1}{2}\|f - g\|_1$ , as required. □

**Proposition 2.** *Let  $f$  be a probability distribution on a finite metric space  $(X, d)$ , and consider its geodesic variance, defined by (8). That is,*

$$\text{Var}(f) = \int_{X \times X} d(x, y)^2 d\mu(x) d\mu(y) = \sum_{x, y \in X} d(x, y)^2 f(x) f(y). \quad (19)$$

*When  $(X, d)$  is a finite subset of the real numbers  $\mathbb{R}$  with its Euclidean metric, this quantity reduces to the classical notion of variance, up to a factor of 2.*

*Proof.* Let  $Y$  be a random variable on  $\mathbb{R}$ . The classical notion of variance is the quantity  $\text{var}(Y) = \mathbb{E} Y^2 - (\mathbb{E} Y)^2$ . If  $Y$  has a distribution  $f$  over a finite set  $X$ , this can be expressed

$$\text{var}(Y) = \sum_{x \in X} x^2 f(x) - \left( \sum_{x \in X} x f(x) \right)^2. \quad (20)$$

On the other hand, (19) can be expanded

$$\text{Var}(f) = \sum_{x,y \in X} (x - y)^2 f(x)f(y) \quad (21)$$

$$= \sum_{x,y \in X} x^2 f(x)f(y) + \sum_{x,y \in X} y^2 f(x)f(y) - 2 \sum_{x,y \in X} xyf(x)f(y) \quad (22)$$

$$= 2 \sum_{x,y \in X} x^2 f(x)f(y) - 2 \sum_{x,y \in X} xyf(x)f(y) \quad (23)$$

$$= 2 \sum_{x \in X} x^2 f(x) - 2 \left( \sum_{x \in X} xf(x) \right) \left( \sum_{y \in X} y^2 f(y) \right) \quad (24)$$

$$= 2\text{var}(Y). \quad (25)$$

Thus, up to a factor of 2, the geodesic variance reduces to the classical notion of variance on the real line. With more care, the same applies if  $X$  is an arbitrary metric space, with  $\nu, \nu$  appropriately integrable measures on  $X$ .  $\square$

---

\* max.menzies@alumni.harvard.edu

- [1] A. Galvani, S. M. Moghadas, and E. C. Schneider, Commonwealth Fund 10.26099/WM2J-MZ32 (2021).
- [2] D. McPhillips and E. Cohen, Uneven vaccination rates across the US linked to Covid-19 case trends, worry experts, <https://edition.cnn.com/2021/05/19/health/uneven-vaccination-rates-covid-19-trends/index.html> (2021), CNN, May 19, 2021.
- [3] N. James and M. Menzies, Chaos: An Interdisciplinary Journal of Nonlinear Science **30**, 091102 (2020).
- [4] N. James, M. Menzies, and P. Radchenko, Chaos: An Interdisciplinary Journal of Nonlinear Science **31**, 031105 (2021).
- [5] Y. Zhou *et al.*, Harvard Data Science Review 10.1162/99608f92.79e1f45e (2020).
- [6] B. Gross *et al.*, EPL (Europhysics Letters) **131**, 58003 (2020).
- [7] A. Maiti *et al.*, Sustainable Cities and Society **68**, 102784 (2021).
- [8] R. Paul, A. A. Arif, O. Adeyemi, S. Ghosh, and D. Han, The Journal of Rural Health **36**, 591 (2020).

- [9] Y. Wang, Y. Liu, J. Struthers, and M. Lian, *Clinical Infectious Diseases* **72**, 643 (2020).
- [10] J. Zheng *et al.*, *Physics of Fluids* **33**, 046605 (2021).
- [11] M. C. Castro *et al.*, *Science* **372**, 821 (2021).
- [12] Y. Feng *et al.*, *PLOS ONE* **15**, e0244351 (2020).
- [13] N. James and M. Menzies, *Physica D: Nonlinear Phenomena* **425**, 132968 (2021).
- [14] N. James and M. Menzies, *Physica D: Nonlinear Phenomena* **417**, 132809 (2021).
- [15] C. S. Ng *et al.*, *Physical Review Fluids* **6**, 054303 (2021).
- [16] O. McRae, K. R. Mead, and J. C. Bird, *Physical Review Fluids* **6**, L031601 (2021).
- [17] S. Verma, M. Dhanak, and J. Frankenfield, *Physics of Fluids* **32**, 091701 (2020).
- [18] F. Yang, A. A. Pahlavan, S. Mendez, M. Abkarian, and H. A. Stone, *Physical Review Fluids* **5**, 122501(R) (2020).
- [19] M. Abkarian and H. A. Stone, *Physical Review Fluids* **5**, 102301(R) (2020).
- [20] R. S. Ganti and A. K. Chakraborty, *Physical Review E* **103**, 052408 (2021).
- [21] G. F. de Arruda, G. Petri, and Y. Moreno, *Physical Review Research* **2**, 023032 (2020).
- [22] Y. Luo and L. P. Schaposnik, *Physical Review Research* **2**, 023001 (2020).
- [23] G. F. de Arruda, G. Petri, F. A. Rodrigues, and Y. Moreno, *Physical Review Research* **2**, 013046 (2020).
- [24] S. Moore and T. Rogers, *Physical Review Letters* **124**, 068301 (2020).
- [25] C. Castellano and R. Pastor-Satorras, *Physical Review X* **10**, 011070 (2020).
- [26] D. H. Silva, S. C. Ferreira, W. Cota, R. Pastor-Satorras, and C. Castellano, *Physical Review Research* **1**, 033024 (2019).
- [27] G. F. de Arruda, E. Cozzo, T. P. Peixoto, F. A. Rodrigues, and Y. Moreno, *Physical Review X* **7**, 011014 (2017).
- [28] L. V. Kantorovich and G. Rubinstein, *Vestnik Leningradskogo Universiteta* **13**, 52 (1958).
- [29] Coronavirus (Covid-19) data in the United States, <https://github.com/nytimes/covid-19-data> (2021), The New York Times, Accessed July 24, 2021.
- [30] Dataset publishing language, [https://developers.google.com/public-data/docs/canonical/states\\_csv](https://developers.google.com/public-data/docs/canonical/states_csv) (2021), Google, Accessed July 24, 2021.